

# Ideal intersections for radio-frequency trap networks

J. H. Wesenberg\*

*Department of Materials, University of Oxford, Oxford OX1 3PH, United Kingdom*

(Dated: October 12, 2018)

We investigate the possible form of ideal intersections for two-dimensional rf trap networks suitable for quantum information processing with trapped ions. We show that the lowest order multipole component of the rf field that can contribute to an ideal intersection is a hexapole term uniquely determined by the tangents of the intersecting paths. The corresponding ponderomotive potential does not provide any confinement perpendicular to the paths if these intersect at right angles, indicating that ideal right-angle X-intersections are impossible to achieve with hexapole fields. Based on this result, we propose an implementation of an ideal oblique-X intersection using a three-dimensional electrode structure.

PACS numbers: 37.10.Gh, 37.10.Ty, 41.20.Cv

Intersections between network paths are a key ingredient in two-dimensional (2D) rf trap networks which have been proposed to allow large scale quantum information processing (QIP) with trapped ions [1, 2, 3]. RF traps confine ions by a combination of rf and quasistatic electric fields [4, 5] and in an ideal network the rf field and the associated ponderomotive potential vanish in the trapping zones and on dedicated paths between zones but nowhere else. Such ideal trap networks have been demonstrated in one dimension (1D) with segmented linear rf traps where transport as well as splitting and joining of groups of ions have been demonstrated to be possible with a very high degree of control [6, 7, 8]. In contrast, no ideal 2D trap networks have been identified, although a number of possible intersection geometries for 2D trap networks have been investigated [9, 10, 11, 12, 13, 14]. The observed shortcomings fall in two broad categories. For T [9], Y [13, 15] and some X [10, 11], intersections, a residual rf field is observed in the paths through the intersection which can possibly lead to motional heating [16], in addition to complicating or hindering controlled ion transport [12]. In contrast, some high-symmetry X geometries offer truly field-free paths but fail to be “fully confining” in the sense that there are unwanted lines of zero field allowing ions to escape the trap network [11].

In this paper we show that the unique simplest form of an ideal intersection for 2D trap networks is an oblique X and propose an implementation of this intersection based on a three-dimensional (3D) electrode structure that faithfully implements the ideal intersection.

The paper is structured as follows: Sec. I defines the basic problem of designing ideal rf trap intersections. In Sec. II we constructively identify a hexapole term uniquely determined by the intersection angle as the only multipole term of hexapole or lower order which can contribute to a zero-field intersection. In Sec. III we investigate the properties of the identified hexapole intersection and show that fully confining hexapole intersections are

only possible at oblique intersection angles. Lastly, in Sec. IV we describe an implementation of the ideal intersection based on a 3D electrode structure.

## I. RF TRAP NETWORKS

Although rf traps use a combination of quasistatic and rf electrical fields to confine charged particles, we will here only be concerned with the rf component. For typical QIP ion traps, the dimensions ( $< \text{mm}$ ) and rf frequencies ( $> \text{MHz}$ ) are such that we can adequately treat the rf field as quasistatic and express the time dependent rf field as  $\cos(\Omega t) \mathbf{E}(\mathbf{r})$ , where  $\Omega$  and  $\mathbf{E}$  denote the rf frequency and spatially varying amplitude, respectively. The rf period  $2\pi/\Omega$  is made to be the fastest time scale of the trap, so that in the adiabatic limit the effect of the field can be described by an external ponderomotive potential  $U$  given by

$$U(\mathbf{r}) \equiv \frac{Q^2}{4M\Omega^2} |\mathbf{E}(\mathbf{r})|^2, \quad (1)$$

where  $M$  and  $Q$  denote the mass and charge of the trapped particle [17, 18]. For the purpose of this paper, it suffices to note that  $U(\mathbf{r})$  is proportional to the square of the local rf field amplitude. Since confinement by electrostatic fields is impossible, the rf field must always be present to allow trapping, and we will assume  $\mathbf{E}(\mathbf{r})$  to be constant as is usually the case in QIP ion traps. In this case,  $U$  constitutes a constant “landscape” in which ions can be shuffled around by manipulating a quasistatic control field provided by dedicated trap electrodes. As mentioned above, we are here only interested in the structure of this landscape, which is determined entirely by the electrode geometry and is independent of the amplitude and frequency of the applied rf field.

For an ideal trap network, as introduced in the Introduction, we require that the  $\mathbf{E}(\mathbf{r})$  vanishes for  $\mathbf{r}$  on a network path and only there. Ideal networks have a number of qualities. Firstly, the ions do not experience any rf-induced micromotion. Micromotion is especially

---

\*janus.wesenberg@materials.ox.ac.uk

critical in trap regions where gate operations are performed [19], but could also potentially lead to heating effects [16]. Secondly, the ponderomotive potential associated with a nonzero rf field along trap paths complicates fully controlled ion transport because the applied control fields must be engineered to compensate for any curvature of  $U$  along the path in order to avoid motional heating of the ions [8, 12]. Note that such compensation is impossible for the transport of multispecies crystals, which according to Eq. (1) experience different ponderomotive potentials due to mass differences. Lastly, the requirement that  $U(\mathbf{r})$  vanishes only on the network paths ensures that ions are confined, even in the absence of control fields.

An ideal 1D trap network can be implemented with segmented linear rf traps [6] where the rf field forms a quadrupole with a line of zero rf field along the trap axis [20], so that the isosurfaces of  $U$  are concentric cylinders around the axis. In this case, transport as well as splitting and joining of groups of ions have been demonstrated to be possible with a very high degree of control [6, 7, 8].

We should note that although our quest in the following is for ideal trap networks, none of the conditions for a network to be ideal in the sense introduced above are absolute requirements for a network to be suitable for even large scale QIP. Firstly, it has been proposed that transport in a network that is not fully confining can be achieved by “surfing” around any leaks [12]. Secondly, even in the presence of residual a rf field along the network path, it can be possible to perform highly controlled ion transport so that no or minimal heating takes place [8, 12]. Nevertheless, it seems that an ideal network would have a number of operational benefits.

## II. UNIQUE HEXAPOLE INTERSECTION

As a first step to constructing an ideal 2D intersection, we will study the possible local structure of  $\mathbf{E}(\mathbf{r})$  at the intersection of two smooth network paths in terms of a multipole expansion. Our goal is to find the lowest order multipole term that can contribute to  $\mathbf{E}(\mathbf{r})$ . Identifying the lowest possible multipole order is desirable for two reasons. Firstly, the confinement that can be produced for a given ion-electrode distance is stronger for lower-order multipole fields [15]. Keeping the ion-electrode distance as large as possible is important since ion heating has been repeatedly demonstrated to increase dramatically with decreasing ion-electrode distance [21, 22, 23]. Secondly, the construction of an intersection where all low-order multipole terms vanish is technically challenging. By trapping with the lowest order multipole possible, a smaller number of terms must be made to vanish.

With this in mind, we expand  $\mathbf{E}(\mathbf{r})$  around the intersection point chosen as the origin,

$$E_i = d_i + q_{i,j}r_j + \frac{1}{2}h_{i,j,k}r_jr_k + \mathcal{O}(\mathbf{r}^3), \quad (2)$$

where the tensors  $q_{i,j} = \partial_j E_i$  and  $h_{i,j,k} = \partial_j \partial_k E_i$  de-

scribe the quadrupole and hexapole components of the field. Here, as in the remainder of the paper, we have adopted the convention that summation over repeated indices is implied, e.g.  $q_{i,j}r_j = q_{i,1}x + q_{i,2}y + q_{i,3}z$ .

It follows from Maxwell’s equations that  $\mathbf{E}(\mathbf{r})$  must be irrotational and divergence-free in the trap region, i.e.,  $\nabla \times \mathbf{E}(\mathbf{r}) = \mathbf{0}$  and  $\nabla \cdot \mathbf{E}(\mathbf{r}) = 0$ . These requirements give rise to constraints on the quadrupole and hexapole tensors. To find these constraints, we note that the requirements are equivalent to requiring that  $\mathbf{E}(\mathbf{r}) = -\nabla V(\mathbf{r})$  for an electric potential  $V$  fulfilling the Laplace condition  $\partial_i \partial_i V(\mathbf{r}) = 0$ . For the quadrupole terms, this implies that  $q_{i,j}$  must be symmetric and traceless,

$$q_{i,j} = q_{j,i} \quad \text{and} \quad q_{i,i} = 0. \quad (3)$$

This leaves five free parameters as expected since a basis of the quadrupole field components can be formed from the five second-order spherical harmonics. For the hexapole terms, we find similarly that  $h_{i,j,k}$  must be symmetric, and that the partial traces must vanish since  $\partial_i \partial_j \partial_k V(\mathbf{r}) = \partial_i \nabla^2 V(\mathbf{r})$ ,

$$h_{i,j,k} = h_{i,k,j} = h_{j,i,k} \quad \text{and} \quad h_{i,i,j} = 0. \quad (4)$$

Here, the symmetry requirement leaves ten independent parameters with  $i \leq j \leq k$ , so that after the three partial trace constraints are included, seven free parameters are left as expected.

We will describe the desired paths of zero field through the intersection by two curves  $\gamma^{(l)}(s)$ ,  $l = 1, 2$ , parametrized by path length  $s$ . The requirements that the curves intersect at the origin and that  $\mathbf{E}$  vanishes on the paths can then be expressed as

$$\gamma^{(l)}(0) = \mathbf{0}, \quad (5a)$$

$$\mathbf{E}(\gamma^{(l)}(s)) = \mathbf{0}, \text{ for all } s \text{ and } l = 1, 2. \quad (5b)$$

To establish the resulting constraints on the multipole coefficients of  $\mathbf{E}(\mathbf{r})$ , we will expand  $\mathbf{E}(\gamma^{(l)}(s))$  in  $s$  and look at each order in turn. We will assume that the curves have a parametrization with continuous second-order derivatives. In this case, we can require the curves to be parametrized by path length, so that  $|\partial_s \gamma^{(l)}(s)| = 1$ . Also, according to Eq. (5a) we then have that

$$\gamma^{(l)}(s) = \hat{\mathbf{T}}^{(l)}s + \hat{\mathbf{N}}^{(l)}\kappa^{(l)}s^2 + \mathcal{O}(s^3), \quad (6)$$

where,  $\hat{\mathbf{T}}^{(l)}$  and  $\hat{\mathbf{N}}^{(l)}$  are the tangent and normal vectors of  $\gamma^{(l)}$  at the origin, and  $\kappa^{(l)}$  is the curvature at the same point. Except for the requirement that the tangent and normal vectors are perpendicular unit vectors,  $\hat{\mathbf{T}}^{(l)}$ ,  $\hat{\mathbf{N}}^{(l)}$ , and  $\kappa^{(l)}$  can be chosen freely.

Let us now assume that  $\mathbf{E}(\gamma^{(l)}(s)) = \mathbf{0}$  as required by Eq. (5b) and deduce the possible value of the multipole expansion coefficients appearing in Eq. (2). Inserting  $\gamma^{(l)}$  in the form Eq. (6) into the expansion of  $\mathbf{E}$  as given by Eq. (2), we find that

$$E_i(\gamma^{(l)}(s)) = d_i + \mathcal{O}(s). \quad (7)$$

For  $\mathbf{E}(\boldsymbol{\gamma}^{(l)}(s))$  to vanish to zeroth order in  $s$ , we must consequently have that

$$d_i = 0, \quad (8)$$

so that the homogeneous field component at the origin vanishes. Continuing the expansion of  $E_i(\boldsymbol{\gamma}^{(l)}(s))$ , given that the  $d_i$  fulfill Eq. (8), we find

$$E_i(\boldsymbol{\gamma}^{(l)}(s)) = q_{i,j} \hat{T}_i^{(l)} s + \mathcal{O}(s^2). \quad (9)$$

It follows that for  $\mathbf{E}(\boldsymbol{\gamma}^{(l)}(s))$  to vanish to first order in  $s$ , we must require that  $\hat{\mathbf{T}}^{(l)}$  is an eigenvector of  $q_{i,j}$  with eigenvalue 0 for  $l = 1, 2$ . In the case where  $\hat{\mathbf{T}}^{(1)}$  and  $\hat{\mathbf{T}}^{(2)}$  are linearly independent (the paths are not cotangential at the intersection), it follows from the additional constraint that  $q_{i,j}$  is symmetric and traceless [Eq. (3)] that

$$q_{i,j} = 0. \quad (10)$$

A more detailed argument, presented in the Appendix, shows that the quadrupole components must vanish even in the cotangential case provided the paths are not identical. For now, we assume the dipole and quadrupole terms to vanish as required by Eqs. (8) and (10), so that the expansion of  $E_i(\boldsymbol{\gamma}^{(l)}(s))$  to second order takes the form

$$E_i(\boldsymbol{\gamma}^{(l)}(s)) = \frac{1}{2} h_{i,j,k} \hat{T}_j^{(l)} \hat{T}_k^{(l)} s^2 + \mathcal{O}(s^3). \quad (11)$$

Note that the expansion only depends on the tangent vectors  $\hat{\mathbf{T}}^{(l)}$  of the curves. For algebraic simplicity, we will orient the coordinate system so that

$$\hat{\mathbf{T}}^{(1)} = \cos(\theta) \hat{\mathbf{x}} + \sin(\theta) \hat{\mathbf{y}} \quad (12a)$$

$$\hat{\mathbf{T}}^{(2)} = \cos(\theta) \hat{\mathbf{x}} - \sin(\theta) \hat{\mathbf{y}}, \quad (12b)$$

where  $\theta$  is half the angle between the tangents of the paths at the origin. Without loss of generality we require  $0 < \theta \leq \pi/4$ . In this case, we find by Eq. (11) that

$$E_i(\boldsymbol{\gamma}^{(1)}(s)) - E_i(\boldsymbol{\gamma}^{(2)}(s)) = 2h_{i,1,2} \cos(\theta) \sin(\theta) s^2 + \mathcal{O}(s^3), \quad (13)$$

and consequently require  $h_{i,1,2} = 0$  for  $E_i(\boldsymbol{\gamma}^{(l)})$  to vanish to second order. Similarly, we find that

$$E_i(\boldsymbol{\gamma}^{(1)}(s)) + E_i(\boldsymbol{\gamma}^{(2)}(s)) = [h_{i,1,1} \cos^2(\theta) + h_{i,2,2} \sin^2(\theta)] s^2 + \mathcal{O}(s^3), \quad (14)$$

so that since by Eqs. (4) and (13)  $h_{1,1,2} = h_{1,2,2} = 0$  also  $h_{2,2,2}$  and  $h_{1,1,1}$  must vanish. Taking the partial trace constraint Eq. (4) into account, we find that the only hexapole terms that can be nonzero are  $h_{1,1,3}$ ,  $h_{2,2,3}$ , and  $h_{3,3,3}$ . For these terms we have, according to Eqs. (4) and

(14), that  $\mathbf{E}(\boldsymbol{\gamma}^{(l)}(s))$  vanishes to second order in  $s$  if and only if

$$h_{1,1,3} \cos^2(\theta) + h_{2,2,3} \sin^2(\theta) = 0 \quad (15a)$$

$$h_{1,1,3} + h_{2,2,3} + h_{3,3,3} = 0, \quad (15b)$$

with the unique solution that

$$\begin{pmatrix} h_{1,1,3} \\ h_{2,2,3} \\ h_{3,3,3} \end{pmatrix} = 6 \alpha_X \begin{pmatrix} -\sin^2(\theta) \\ +\cos^2(\theta) \\ \sin^2(\theta) - \cos^2(\theta) \end{pmatrix}, \quad (16)$$

for some constant  $\alpha_X$ . To fulfill the requirements of Eqs. (8), (10), and (16), we find that the electrical potential must be of the form

$$V(\mathbf{r}) = \alpha_X \Theta_X(\mathbf{r}) + \mathcal{O}(r^4), \quad (17)$$

where the basis function  $\Theta_X$  is given by

$$\Theta_X(\mathbf{r}) \equiv \sin^2(\theta) z(3x^2 - z^2) - \cos^2(\theta) z(3y^2 - z^2) \quad (18)$$

$$= \sin^2(\theta) \Theta_X^{(x)}(\mathbf{r}) - \cos^2(\theta) \Theta_X^{(y)}(\mathbf{r}), \quad (19)$$

where we have introduced the basis functions  $\Theta_X^{(i)} \equiv z(3r_i^2 - z^2)$  for later reference.

To summarize, we have constructively established that to form a zero-field intersection,  $\mathbf{E}(\mathbf{r})$  must have vanishing dipole and quadrupole terms. Furthermore, if the intersection is not cotangential, the only possible field configuration is  $\mathbf{E}(\mathbf{r}) = -\alpha_X \nabla \Theta_X(\mathbf{r}) + \mathcal{O}(r^3)$ .

The key assumption in the arguments presented above is that the curves  $\boldsymbol{\gamma}^{(l)}$  have continuous second derivatives, so that the expansion Eq. (6) is valid. We assume it to be the case that all isolated lines of zero field will have this property, but even though the structure of zero-field points in free space electrostatic potentials, or equivalently critical points of harmonic functions, has been intensely studied, most results appear to pertain to 2D systems and we have not found any direct argument to support our assumption, which must consequently stand as a conjecture. On the other hand, we can say for certain that if the field vanishes on an interval of a curve with analytic parametrization, e.g., a straight line segment, then it must vanish everywhere on the analytic continuation of that line segment. This follows from the fact that the maps  $s \rightarrow E_i(\boldsymbol{\gamma}^{(l)}(s))$  will in this case be analytic as long as  $\boldsymbol{\gamma}^{(l)}(s)$  is in free space. This clearly rules out the possibility of ideal straight-line Y or T intersections where a straight line segment with zero field would have to terminate at the intersection point.

Finally, we should point out that a fully confining, zero-field, right-angle intersection does exist. According to the results above, for this case  $V(\mathbf{r})$  must be  $\mathcal{O}(r^4)$ , so that the resulting intersection has a number of disadvantages compared to hexapole intersections as discussed in the beginning of this section. By brute force search in the possible octupole terms we find that  $V(\mathbf{r}) = \alpha_O \Theta_O(\mathbf{r})$  for

$$\Theta_O(\mathbf{r}) = z^4 - 3(x^2 + y^2)z^2 + 3x^2y^2 \quad (20)$$

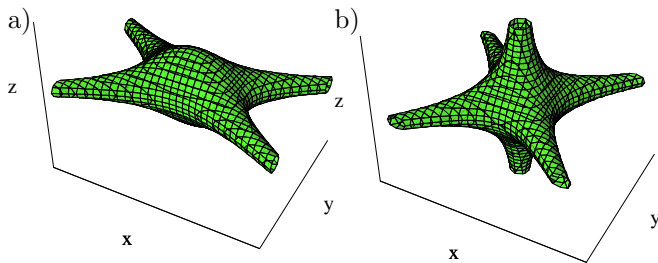


FIG. 1: (Color online) Isosurface of  $|\nabla\Theta_X|^2$  for  $\Theta_X$  of Eq. (17) for  $\theta = \pi/6$  (a) and  $\pi/4$  (b). The isosurface is truncated to a cube: according to Eq. (22) the zero-field lines extend to infinity. Note that there is no confinement along the  $z$  axis for  $\theta = \pi/4$ . Since all terms of  $\Theta_X$  are third order in the coordinates, the isosurfaces of  $|\nabla\Theta_X|^2$  are related by scaling about the origin.

is an example of an octupole potential giving rise to an intersection with zero field on the  $x$  and  $y$  axes but nowhere else.

### III. PROPERTIES OF THE HEXAPOLE INTERSECTION

In this section we investigate the properties of the hexapole intersection described by Eq. (17) in more detail, first with respect to confinement properties and then with respect to implementation considerations.

#### A. Confinement properties

To study the confinement properties of  $U \propto |\nabla\Theta_X|^2$  corresponding to the hexapole field described by  $\Theta_X$ , we look for points where the corresponding field

$$\nabla\Theta_X(\mathbf{r}) = 3 \begin{pmatrix} 2xz \sin^2(\theta) \\ -2yz \cos^2(\theta) \\ (z^2 - y^2) \cos^2(\theta) - (z^2 - x^2) \sin^2(\theta) \end{pmatrix} \quad (21)$$

vanishes. In the general case, this is seen to happen along the two lines

$$y = \pm \tan(\theta)x \quad \text{for } z = 0, \quad (22)$$

which are exactly the tangent lines specified in Eq. (12). However, for the special case of  $\theta = \pi/4$ ,  $\nabla\Theta_X$  also vanishes everywhere on the  $z$  axis, as illustrated in Fig. 1.

To understand the transition to vanishing confinement in the  $z$  direction, we consider the strength of the (quartic) confinement provided by  $U$  along the  $y$  and  $z$  axes as follows:

$$|\nabla\Theta_X|^2 = 9 \begin{cases} y^4 \cos^4(\theta) & \text{for } x = z = 0 \\ z^4 \cos^2(2\theta) & \text{for } x = y = 0. \end{cases} \quad (23)$$

Although confinement strength decreases monotonously with increasing  $\theta$  for both axes, only the  $z$  confinement vanishes completely.

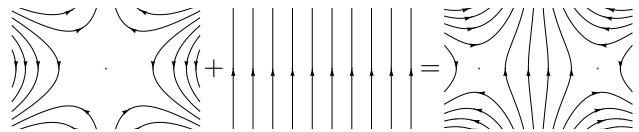


FIG. 2: Field lines of a hexapole and a homogeneous field, together with the field lines of the superposition field which has two quadrupole poles. Reversing the sign of the homogeneous field would shift the two quadrupoles to above and below the hexapole center.

#### B. Implementation considerations

One reason that low-order intersections are interesting is that in practical implementations, it is difficult to passively ensure that all lower-order terms vanish exactly. For typical traps with nonadjustable electrode geometry and a single rf feed only the strength and frequency of the rf field can be changed once the trap is in its operational configuration. The geometry of the rf field, including the relative strength of the multipole terms at the intersection point, is not adjustable for such traps. Since lower-order terms dominate at the intersection point, this could be critical to the performance of the intersection. We will consequently investigate which lower-order terms are allowed by symmetry and try to describe the perturbing effects of these on the hexapole intersection, Eq. (17).

Let us first note that the hexapole intersection potential described by  $\Theta_X(\mathbf{r})$  is symmetric in  $x$  and  $y$  and antisymmetric in  $z$ ,

$$\Theta_X(x, y, z) = \Theta_X(-x, y, z) = \Theta_X(x, -y, z), \quad (24a)$$

$$\Theta_X(x, y, z) = -\Theta_X(x, y, -z). \quad (24b)$$

An analysis similar to that of Sec. II shows that these symmetry requirements alone constrain  $V$  to be of the form

$$V(\mathbf{r}) = \alpha_H z + \alpha_X \Theta_X(\mathbf{r}) + \mathcal{O}(r^4) \quad (25)$$

for some constant  $\alpha_H$ . Under the generous assumption that an implementation exactly obeys the symmetries, Eq. (24), the only possible deviation from the ideal intersection given by Eq. (17) is consequently a homogeneous field in the  $z$  direction. To empirically design a zero-field intersection under this symmetry, it is thus sufficient to ensure that the field vanishes at the intersection point, so that  $\alpha_H = 0$ .

In realistic implementations, any field component not explicitly disallowed by symmetry would most likely be nonzero. It is consequently of interest to investigate the properties of  $U$  corresponding to the form of  $V$  given by Eq. (25) for small nonzero values of  $\alpha_H$ . An intuitive understanding of the effects of a perturbing homogeneous field can be had by considering the form of  $\nabla\Theta_X$  in the  $y$ - $z$  plane. Here by Eq. (21),

$$\nabla\Theta_X(\mathbf{r}) = 3 \begin{pmatrix} 0 \\ -2yz \cos^2(\theta) \\ z^2 \cos(2\theta) - y^2 \cos^2(\theta) \end{pmatrix} \text{ for } x = 0, \quad (26)$$

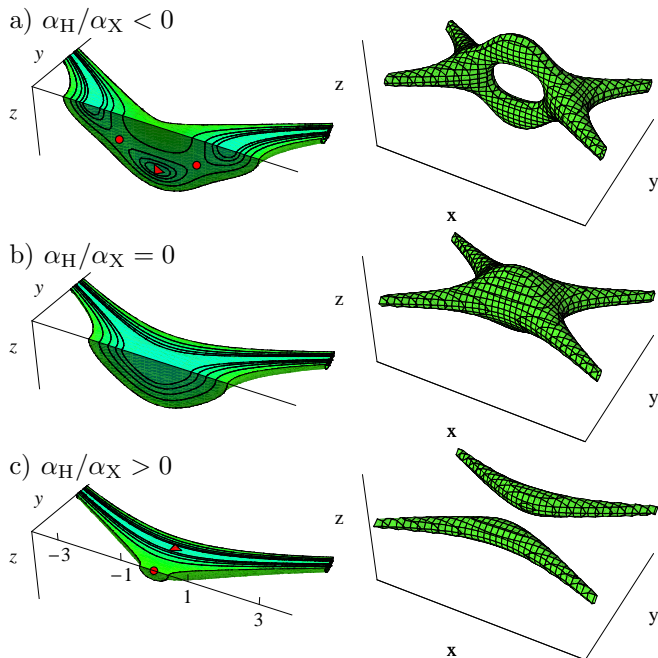


FIG. 3: (Color online) Intersection structure modifications in the presence of a homogeneous field component, as described by  $\alpha_H \neq 0$  in Eq. (25). Left-hand column: Contour curves of  $|\nabla(\alpha_H z + \alpha_X \Theta_X)|^2$  on  $x$ - $y$  and  $x$ - $z$  cut planes. Circles mark the barriers with a position given by Eq. (29) for  $\alpha_H/\alpha_X < 0$ , triangles mark the field zeros in the  $y$ - $z$  plane as described by Eq. (27). The length scale is  $\sqrt{|\alpha_H/3\alpha_X|}$  and  $\theta = \pi/6$ . Right-hand column: Full 3D form of the next-to-outermost contour. Note that in all three cases the outermost contour is connected and confined transport between any of the intersection entries is possible although the height of the barriers (circles) differs as discussed in the text.

describing a deformed in-plane hexapole field. As illustrated by Fig. 2, a homogeneous field will split a hexapole field into two quadrupoles. For a field of the form given by Eq. (25), the positions of these quadrupole field zeros are

$$\sqrt{\frac{|\alpha_H|}{3|\alpha_X|}} \begin{cases} \pm \sec(\theta) \hat{\mathbf{y}} & \text{for } \alpha_H/\alpha_X \geq 0 \\ \pm \sqrt{\sec(2\theta)} \hat{\mathbf{z}} & \text{for } \alpha_H/\alpha_X \leq 0. \end{cases} \quad (27)$$

The positions are seen to depend critically on the sign of  $\alpha_H$ . For  $\alpha_H/\alpha_X > 0$ , the zeros are located on the  $y$ -axis, while for  $\alpha_H/\alpha_X < 0$  they are located on the  $z$ -axis.

The global shape of the intersection described by  $V(\mathbf{r}) = \alpha_H z + \alpha_X \Theta_X(\mathbf{r})$  is very different in these two cases as illustrated by Fig. 3. For  $\alpha_H/\alpha_X < 0$ , we get a double-junction structure with two junctions on the  $x$  axis, connected by paths in the  $x$ - $z$  plane. The field is zero on the paths in the  $x$ - $y$  plane, but this is not the case for the paths joining the junctions where we find barriers with a maximum height of

$$|\nabla V|^2 = \alpha_H^2 \tan^2(\theta), \quad (28)$$

located at the four points (all sign combinations)

$$\sqrt{\frac{|\alpha_H|}{6|\alpha_X|}} \left( \pm \sqrt{\csc^2(\theta) - \sec^2(\theta)} \hat{\mathbf{x}} \pm \sec(\theta) \hat{\mathbf{z}} \right). \quad (29)$$

This structure is similar to that described in Refs. [24, 25]. For  $\alpha_H/\alpha_X > 0$ , we get two disjoint paths through the intersection. The height of the barrier at the origin is

$$|\nabla V|^2 = \alpha_H^2, \quad (30)$$

corresponding to the ponderomotive potential due to the homogeneous field component.

Given a certain production tolerance, Eqs. (28) and (30) show that it is beneficial to aim for a negative value of  $\alpha_H/\alpha_X$ , corresponding to the double-junction configuration. For a given value of  $|\alpha_H|$ , this will reduce the barrier height by a factor of  $\tan^2(\theta)$  compared to the case of  $\alpha_H/\alpha_X > 0$ .

#### IV. IMPLEMENTATION WITH 3D ELECTRODE STRUCTURE

We will now describe a 3D electrode structure that can be used to implement the ideal intersection described by Eq. (17).

Firstly, we note that the full symmetry of  $\Theta_X$  as described by Eq. (24) can be retained in an implementation based on a 3D configuration of electrodes as illustrated in Fig. 4. According to the results of the previous section, it follows that the potential at the origin must be of the form given by Eq. (25). In addition, it turns out, the symmetry ensures unbroken lines of zero field in the  $x$ - $y$  plane. By Eq. (24) the field in the  $x$ - $y$  plane will be odd in  $z$ . Furthermore, the  $z$  component of the field in the  $x$ - $y$  plane is a continuous function of  $x$  and  $y$  and the zero contour of this function, consisting of unbroken lines, will define the points of zero field.

In total, these properties ensure that it is relatively easy to design a zero-field intersection using 3D electrodes: After choosing an overall design that ensures that there are paths of zero field leaving the intersection point, all that remains is to ensure that  $\alpha_H \equiv -E_z(\mathbf{0}) = 0$ . In the implementation illustrated in Fig. 4, this was achieved by a bisecting search for the correct value of a single dimensional parameter.

It should be noted that symmetry alone does not define the angle  $\theta$  between the intersecting paths, but rather constrains the hexapole component to be a superposition of two components  $\Theta_X^{(x)}(\mathbf{r})$  and  $\Theta_X^{(y)}(\mathbf{r})$  as follows:

$$V(\mathbf{r}) = \alpha_X^{(x)} \Theta_X^{(x)}(\mathbf{r}) + \alpha_X^{(y)} \Theta_X^{(y)}(\mathbf{r}). \quad (31)$$

For the implementation illustrated in Fig. 4, we numerically find that  $\alpha_X^{(x)} = 0.011 V_0/d^3$  and  $\alpha_X^{(y)} = 0.12 V_0/d^3$ ,

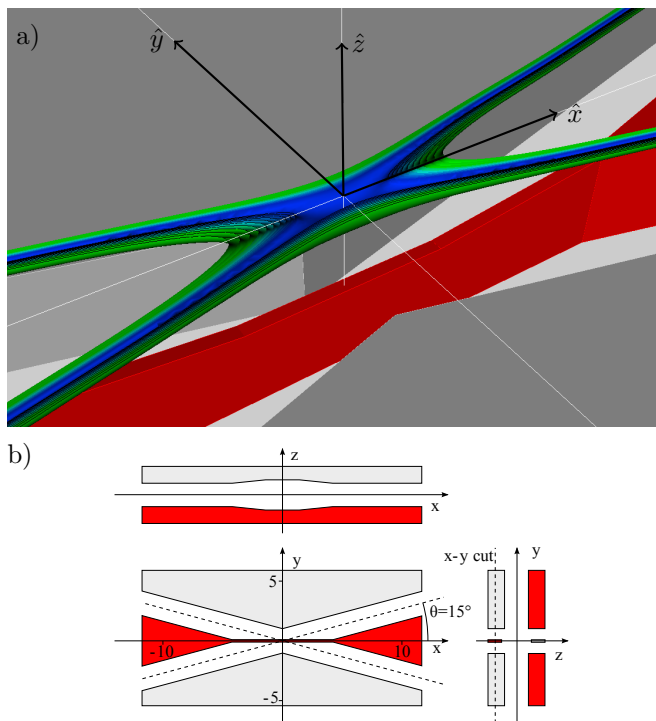


FIG. 4: (Color online) Example implementation of an ideal intersection using a 3D electrode structure. (a) 3D view of the electrodes (red and gray polygons) and isosurfaces of  $|\nabla V(\mathbf{r})|^2$  (blue to green curved surfaces) with all components with  $z > 0$  cut away. (b) Cuts through the electrode structure, which is symmetric under inversion in the  $x$ - $z$  and  $y$ - $z$  planes, and antisymmetric under inversion in the  $x$ - $y$  to maintain the symmetry of  $\Theta_X$  as described by Eq. (24). Units are the ion-electrode distance  $d$ . Results are based on numerical simulations performed using the CPO program [26].

where  $V_0$  is the peak amplitude of the applied rf and  $d$  is the distance from the trap center to the nearest electrode. These values correspond to the rf field being described by Eq. (17) with a strength of  $\alpha_X = 0.13 V_0/d^3$  and an angle of  $\theta = \arctan(\sqrt{\alpha_X^{(x)}/\alpha_X^{(y)}}) = 17^\circ$ . The obtained strength seems reasonable, given that the strongest possible hexapole guides along the  $x$  or  $y$  axes would correspond to  $\alpha_X^{(x/y)} = \frac{1}{2} V_0/d^3$  [15]. The angle is relatively close to the asymptotic angle of  $\theta = 15^\circ$  chosen for the demonstration design. If better agreement was desired, an additional fit parameter (for example, the length of the bridge recession) could have been included to ensure that the unwanted hexapole component  $\cos^2(\theta)\Theta_X^{(x)} + \sin^2(\theta)\Theta_X^{(y)}$  associated with a given value of  $\theta$  was made to vanish.

## V. CONCLUSIONS AND OUTLOOK

In conclusion, we have shown that a zero-field intersection for rf traps cannot have any field component of

quadrupole or lower order at the intersection point. Furthermore, we have demonstrated that the hexapole field component at the intersection point is uniquely determined by the intersection angle [Eq. (17)], and that this component does not provide any confinement perpendicular to the intersecting paths if these intersect at right angles. These results can serve as a guide for the design of intersections for rf trap networks suitable for QIP based on trapped ions. We have suggested how the intersection could be implemented using 3D electrodes. In relation to implementations of the intersection, we have shown that if static field components cannot be guaranteed to completely vanish at the intersection point, it is beneficial to ensure that the imperfect intersection is of the “double-junction” type [Fig. 3 (a)].

The proposed implementation of the ideal intersection illustrated in Fig. 4 is not well suited for microfabrication, which would most likely be a requirement for fabrication of large scale trap networks. For this reason it would be worthwhile to find intersection implementations with electrode geometries better suited for microfabrication, such as the surface-electrode geometry [11], which is compatible with large scale microfabrication [27], and has the lowest demonstrated heating rates for microfabricated traps [23, 28, 29]. Initial investigations in this direction indicate that such intersections need to be very oblique ( $\theta \approx \pi/12$ ) to obtain reasonable hexapole strengths for an intersection of two straight guides. As an alternative, it might be worthwhile to investigate cotangential intersections of curved guides.

## Acknowledgments

We thank J. Amini, D. Leibfried, and D. Wineland for stimulating discussions. This work was supported by the Danish National Research Agency, the Carlsberg Foundation, and the QIP IRC (Grant No. GR/S82176/01).

## APPENDIX A: GENERAL PROOF OF ABSENCE OF QUADRUPOLE TERMS IN AN INTERSECTION

Here we present a general proof that there can be no quadrupole terms in the multipole expansion of  $\mathbf{E}$  as given by Eq. (2), even in the cotangential case where  $\hat{\mathbf{T}}^{(1)} = \hat{\mathbf{T}}^{(2)}$ , provided that the paths  $\gamma^{(l)}$  have analytic parametrizations and are not identical.

We expand the paths as

$$\gamma^{(1)}(s) = \sum_{n=1}^{\infty} \mathbf{u}^{(n)} s^n \quad (\text{A1a})$$

$$\gamma^{(2)}(s) = \sum_{n=1}^{\infty} \mathbf{v}^{(n)} s^n, \quad (\text{A1b})$$

where in particular  $\mathbf{u}^{(1)} = \hat{\mathbf{T}}^{(1)}$  and  $\mathbf{v}^{(1)} = \hat{\mathbf{T}}^{(2)}$  are the identical tangent vectors. We now take  $M$  to be the

smallest integer so that  $\mathbf{u}^{(M)} \neq \mathbf{v}^{(M)}$ . Such an  $M$  must exist since the paths are assumed not to be identical. Assume as in Sec. II that  $\mathbf{E}(\gamma^{(l)}(s)) = \mathbf{0}$  for all  $s$  so that by Eq. (8),  $d_i = 0$ . We then find that

$$E_i(\gamma^{(1)}(s)) - E_i(\gamma^{(2)}(s)) = q_{i,j} \left( u_j^{(M)} - v_j^{(M)} \right) s^M + \mathcal{O}(s^{M+1}), \quad (\text{A2})$$

so that for the difference to vanish to  $M$ -th order, we must have

$$\mathbf{u}^{(M)} - \mathbf{v}^{(M)} \in N_q, \quad (\text{A3})$$

where  $N_q$  is the null space of the  $q$  tensor. As in the noncotangential case, we have from Eq. (9) that

$$\mathbf{u}^{(1)} = \mathbf{v}^{(1)} \in N_q. \quad (\text{A4})$$

On the other hand, letting  $\bar{\gamma}(s) = \sum_{n < M} \mathbf{u}^{(n)} s^n$  we have that

$$\left| \partial_s \gamma^{(1)}(s) \right|^2 = \left| \partial_s \bar{\gamma}(s) \right|^2$$

$$+ 2\mathbf{u}^{(1)} \cdot \mathbf{u}^{(M)} s^{M-1} + \mathcal{O}(s^M), \quad (\text{A5a})$$

$$\left| \partial_s \gamma^{(2)}(s) \right|^2 = \left| \partial_s \bar{\gamma}(s) \right|^2 + 2\mathbf{v}^{(1)} \cdot \mathbf{v}^{(M)} s^{M-1} + \mathcal{O}(s^M). \quad (\text{A5b})$$

Taking the difference, we find by Eq. (A4)

$$\left| \partial_s \gamma^{(1)}(s) \right|^2 - \left| \partial_s \gamma^{(2)}(s) \right|^2 = 2\mathbf{u}^{(1)} \cdot \left( \mathbf{u}^{(M)} - \mathbf{v}^{(M)} \right) s^{M-1} + \mathcal{O}(s^M), \quad (\text{A6})$$

so that for the difference to vanish, which it must since both curves are parametrized by path length, we must have

$$\mathbf{u}^{(1)} \cdot \left( \mathbf{u}^{(M)} - \mathbf{v}^{(M)} \right) = 0, \quad (\text{A7})$$

so that  $\mathbf{u}^{(1)}$  and  $\mathbf{u}^{(M)} - \mathbf{v}^{(M)}$  are linearly independent. As  $\mathbf{u}^{(1)}$  and  $\mathbf{u}^{(M)} - \mathbf{v}^{(M)}$  are both non-zero and by Eqs. (A3) and (A4) members of  $N_q$ , it follows that  $q_{i,j} = 0$  since  $q_{i,j}$  is symmetric and traceless.

- 
- [1] C. Ospelkaus, C. E. Langer, J. M. Amini, K. R. Brown, D. Leibfried, and D. J. Wineland, "Trapped-ion quantum logic gates based on oscillating magnetic fields," *Phys. Rev. Lett.* **101** (2008) 090502.
- [2] D. Kielpinski, C. Monroe, and D. J. Wineland, "Architecture for a large-scale ion-trap quantum computer," *Nature* **417** (2002) 709.
- [3] D. Leibfried, E. Knill, C. Ospelkaus, and D. J. Wineland, "Transport quantum logic gates for trapped ions," *Phys. Rev. A* **76** (2007) 032324.
- [4] E. Fischer, "Die dreidimensionale stabilisierung von ladungstragern in einem vierpolfeld," *Z. Phys.* **156** (1959) 1–26.
- [5] R. F. Wuerker, H. Shelton, and R. V. Langmuir, "Electrodynamic containment of charged particles," *J. Appl. Phys.* **30** (1959) 342–349.
- [6] M. A. Rowe, A. Ben-Kish, B. DeMarco, D. Leibfried, V. Meyer, J. Beall, J. Britton, J. Hughes, W. M. Itano, B. Jelenkovic, C. Langer, T. Rosenband, and D. J. Wineland, "Transport of quantum states and separation of ions in a dual rf ion trap," *Quantum Inf. Comput.* **2** (2002) 257.
- [7] M. D. Barrett, J. Chiaverini, T. Schaetz, J. Britton, W. M. Itano, J. D. Jost, E. Knill, C. Langer, D. Leibfried, R. Ozeri, and D. J. Wineland, "Deterministic quantum teleportation of atomic qubits," *Nature* **429** (2004) 737.
- [8] R. Reichle, A. Leibfried, R. B. Blakestad, J. Britton, J. D. Jost, E. Knill, C. Langer, R. Ozeri, S. Seidelin, and D. J. Wineland, "Transport dynamics of single ions in segmented microstructured paul trap arrays," *Fortschr. Phys.* **54** (2006) 666–685.
- [9] W. K. Hensinger, S. Olmschenk, D. Stick, D. Hucul, M. Yeo, M. Acton, L. Deslauriers, C. Monroe, and J. Rabchuk, "T-junction ion trap array for two-dimensional ion shuttling, storage, and manipulation," *Appl. Phys. Lett.* **88** (2006) 34101.
- [10] C. E. Pearson, D. R. Leibbrandt, W. S. Bakr, W. J. Mallard, K. R. Brown, and I. L. Chuang, "Experimental investigation of planar ion traps," *Phys. Rev. A* **73** (2006) 032307.
- [11] J. Chiaverini, R. B. Blakestad, J. Britton, J. D. Jost, C. Langer, D. Leibfried, R. Ozeri, and D. J. Wineland, "Surface-electrode architecture for ion-trap quantum information processing," *Quantum Inf. Comput.* **5** (2005) 419.
- [12] D. Hucul, M. Yeo, W. K. Hensinger, J. Rabchuk, S. Olmschenk, and C. Monroe, "On the transport of atomic ions in linear and multidimensional ion trap arrays," *Quantum Inf. Comput.* **8** (2008) 0501–0578. <http://www.rintonpress.com/journals/qicabstracts/qicabstracts8-67.html>.
- [13] J. Amini, S. Seidelin, J. Wesenberg, J. Britton, B. Blakestad, K. Brown, R. Epstein, J. Home, J. Jost, C. Langer, D. Leibfried, R. Ozeri, and D. Wineland, "Multilayer Interconnects for Microfabricated Surface Electrode Ion Traps." Conference poster, DAMOP 2007, Calgary, Canada, Jun., 2007. <http://meetings.aps.org/link/BAPS.2007.DAMOP.K1.17>.
- [14] J. H. Wesenberg, J. M. Amini, R. B. Blakestad, J. Britton, K. R. Brown, R. J. Epstein, J. P. Home, W. M. Itano, J. D. Jost, C. Langer, D. Leibfried, R. Ozeri, S. Seidelin, and D. J. Wineland, "Analytical Methods for Design of Surface-Electrode Ion Traps." Conference poster, DAMOP 2007, calgary, canada, Jun., 2007. <http://meetings.aps.org/link/BAPS.2007.DAMOP.K1.12>.
- [15] J. H. Wesenberg, "Electrostatics of surface-electrode ion traps," *Phys. Rev. A* **78** (2008) 063410.
- [16] R. Blümel, C. Kappler, W. Quint, and H. Walther,

- “Chaos and order of laser-cooled ions in a paul trap,” *Phys. Rev. A* **40** (1989) 808.
- [17] H. G. Dehmelt, “Radiofrequency spectroscopy of stored ions i: Storage,” *Adv. At. Mol. Phys* **3** (1967) 53.
- [18] P. K. Ghosh, *Ion Traps*. Clarendon Press, Oxford, 1995.
- [19] D. J. Wineland, C. R. Monroe, W. M. Itano, D. Leibfried, B. E. King, and D. Meekhof, “Experimental issues in coherent quantum-state manipulation of trapped atomic ions,” *J. Res. Natl. Inst. Stand. Technol.* **103** (1998) 259. <http://www.nist.gov/jres>.
- [20] W. Paul, “Electromagnetic traps for charged and neutral particles,” *Rev. Mod. Phys.* **62** (1990) 531–540.
- [21] Q. A. Turchette, D. Kielpinski, B. E. King, D. Leibfried, D. M. Meekhof, C. J. Myatt, M. A. Rowe, C. A. Sackett, C. S. Wood, W. M. Itano, C. Monroe, and D. J. Wineland, “Heating of trapped ions from the quantum ground state,” *Phys. Rev. A* **61** (2000) 063418.
- [22] L. Deslauriers, S. Olmschenk, D. Stick, W. K. Hensinger, J. Sterk, and C. Monroe, “Scaling and suppression of anomalous quantum decoherence in ion traps,” *Phys. Rev. Lett.* **97** (2006) 103007.
- [23] R. J. Epstein, S. Seidelin, D. Leibfried, J. H. Wesenberg, J. J. Bollinger, J. M. Amini, R. B. Blakestad, J. Britton, J. P. Home, W. M. Itano, J. D. Jost, E. Knill, C. Langer, R. Ozeri, N. Shiga, and D. J. Wineland, “Simplified motional heating rate measurements of trapped ions,” *Phys. Rev. A* **76** (2007) 033411.
- [24] D. Cassettari, B. Hessmo, R. Folman, T. Maier, and J. Schmiedmayer, “Beam splitter for guided atoms,” *Phys. Rev. Lett.* **85** (2000) 5483.
- [25] D. Müller, E. A. Cornell, M. Prevedelli, P. D. D. Schwindt, A. Zozulya, and D. Z. Anderson, “Waveguide atom beam splitter for laser-cooled neutral atoms,” *Opt. Lett.* **25** (2000) 1382.
- [26] “Charged Particle Optics.” <http://www.electronoptics.com/>. High precision electrostatic BEM solver.
- [27] J. Kim, S. Pau, Z. Ma, H. R. McLellan, J. V. Gates, A. Kornblit, R. E. Slusher, R. M. Jopson, I. Kang, and M. Dinu, “System design for large-scale ion trap quantum information processor,” *Quantum Inf. Comput.* **5** (2005) 515.
- [28] S. Seidelin, J. Chiaverini, R. Reichle, J. J. Bollinger, D. Leibfried, J. Britton, J. H. Wesenberg, R. B. Blakestad, R. J. Epstein, D. B. Hume, J. D. Jost, C. Langer, R. Ozeri, N. Shiga, and D. J. Wineland, “A microfabricated surface-electrode ion trap for scalable quantum information processing,” *Phys. Rev. Lett.* **96** (2006) 253003.
- [29] J. Labaziewicz, Y. Ge, P. Antohi, D. Leibbrandt, K. R. Brown, and I. L. Chuang, “Suppression of heating rates in cryogenic surface-electrode ion traps,” *Phys. Rev. Lett.* **100** (2008) 013001.